

1 **Zika virus infection induces IL-1 β -mediated inflammatory responses by macrophages in the**
2 **brain of an adult mouse model**

3

4 Running title: ZIKV induces brain inflammation by macrophages

5

6 Gi Uk Jeong,^a Sumin Lee,^{a,*} Do Yeon Kim,^a Jaemyun Lyu,^b Gun Young Yun,^a Junsu Ko,^b Young-
7 Chan Kwon^a

8

9 ^a Department of Convergent Research for Emerging Virus Infection, Korea Research Institute of
10 Chemical Technology, Daejeon 34114, Republic of Korea

11 ^b Arontier Co., Ltd., Seoul 06735, Republic of Korea

12

13 Address correspondence to Young-Chan Kwon, yckwon@kRICT.re.kr

14 Gi Uk Jeong and Sumin Lee contributed equally to this work.

15 *Present address: Sumin Lee, International Vaccine Institute, Seoul, Republic of Korea

16

17 Abstract word count: 224

18 Main text word count: 4125

19

20 **Abstract**

21 During the 2015/16 Zika virus (ZIKV) epidemic, ZIKV associated neurological diseases were
22 reported in adults, including microcephaly, Guillain-Barre syndrome, myelitis, meningoencephalitis,
23 and fatal encephalitis. However, the mechanisms underlying the neuropathogenesis of ZIKV
24 infection are not yet fully understood. In this study, we used an adult ZIKV-infection mouse model
25 (*Ifnar1*^{-/-}) to investigate the mechanisms underlying neuroinflammation and neuropathogenesis.
26 ZIKV infection induced the expression of proinflammatory cytokines, including IL-1 β , IL-6, IFN- γ ,
27 and TNF- α , in the brains of *Ifnar1*^{-/-} mice. RNA-seq analysis of the infected mouse brain also
28 revealed that genes involved in innate immune responses and cytokine-mediated signaling pathways
29 were significantly upregulated at 6 days post infection. Furthermore, ZIKV infection induced
30 macrophage infiltration and activation, and augmented IL-1 β expression, whereas microgliosis was
31 not observed in the brain. Using human monocyte THP-1 cells, we confirmed that ZIKV infection
32 promotes inflammatory cell death and increases IL-1 β secretion. In addition, the expression of
33 complement component C3, which is associated with neurodegenerative diseases and known to be
34 upregulated by proinflammatory cytokines, was induced by ZIKV infection through the IL-1 β -
35 mediated pathway. An increase in C5a produced by complement activation in the brains of ZIKV-
36 infected mice was also confirmed. Taken together, our results suggest that ZIKV infection of the
37 brain in this animal model augments IL-1 β expression in infiltrating macrophages and elicits IL-1 β -
38 mediated inflammation, which can lead to the destructive consequences of neuroinflammation.

39

40

41 **Importance**

42 Zika virus (ZIKV) associated neurological impairments are an important global health problem. Our
43 results suggest that ZIKV infection of the mouse brain can induce IL-1 β -mediated inflammation and
44 complement activation, contributing to the development of neurological disorders. Thus, our findings
45 reveal a mechanism by which ZIKV induces neuroinflammation in the mouse brain. Although we
46 used adult type I IFN receptor IFNAR knockout (*Ifnar1*^{-/-}) mice owing to the limited mouse model
47 of ZIKV pathogenesis, our conclusion could contribute to understanding ZIKV associated
48 neurological diseases to develop treatment strategies based on these findings for the patients with
49 ZIKV infection.

50

51 **Keywords**

52 Zika virus, IL-1 β , macrophage, neuroinflammation, Complement C3

53

54 Introduction

55 During the 2015/16 epidemic of Zika virus (ZIKV) in the Americas (1), case reports indicated an
56 association between congenital ZIKV infection and microcephaly (2, 3). The rapid spread of ZIKV
57 has also indicated a causal relationship between ZIKV infection and neurological complications in
58 adults, including Guillain-Barré syndrome (GBS) (4), myelitis (5), meningoencephalitis (6), and fatal
59 encephalitis (7), suggesting a possible association between ZIKV and neurological diseases. Limb
60 weakness, hyporeflexia/areflexia, facial palsy, and paresthesia are the most frequent neurological
61 symptoms in patients with ZIKV-associated GBS (8). However, the neuropathogenesis of ZIKV
62 infection is not yet fully understood.

63 ZIKV belongs to the *Flaviviridae* family of RNA viruses and is a neurotropic flavivirus, along with
64 Japanese encephalitis and West Nile viruses (9). The detection of ZIKV RNA in the brains and
65 cerebrospinal fluid of adult patients with ZIKV-induced neurological disorders also suggests a
66 neuroinvasive characteristic of ZIKV (6, 10-13). ZIKV can infect human neuronal progenitor cells
67 (NPCs), leading to cell death and abnormal growth (14, 15). ZIKV infection of NPCs in the adult
68 mouse brain results in cell death and reduced proliferation (16). In addition to NPCs, human
69 placental macrophages (17) and glial cells (18) are also susceptible to ZIKV infection. Lum et al.
70 demonstrated that ZIKV infects human fetal brain microglia and macrophages, which induces high
71 levels of proinflammatory cytokines; these are implicated in ZIKV-derived neuroinflammation (19).
72 Increasing evidence indicates that neuroinflammation is a major contributor to the pathogenesis of
73 neurological diseases (20). Thus, an investigation to address the mechanisms underlying the
74 neuropathogenesis of ZIKV infection would help to understand ZIKV-associated neurological
75 diseases.

76 Proinflammatory cytokines are central mediators of the inflammatory response. Interleukin (IL)-1 β is
77 one of the most extensively studied cytokines involved in neuroinflammation and neurodegenerative

78 diseases (21). In the brains of patients with human immunodeficiency virus 1 encephalitis, IL-1 β
79 expression is increased in infiltrating macrophages, microglia, and astrocytes (22, 23). Complement
80 component 3 (C3) is also induced in neurodegenerative diseases and is upregulated by
81 proinflammatory cytokines such as IL-1 β , interferon (INF)- γ , and tumor necrosis factor (TNF)- α (24-
82 27). Simian immunodeficiency virus infection of the central nervous system (CNS) in rhesus
83 macaques induces C3 expression in infiltrating macrophages, astrocytes, and neurons (28). Although
84 both IL-1 β and C3 can play neuroprotective roles in immune responses, uncontrolled biosynthesis
85 and activation can lead to critical brain tissue damage (24, 29). Hence, whether IL-1 β and C3
86 expression in the brain is affected by ZIKV infection needs to be investigated to explore ZIKV-
87 associated neurological diseases.

88 Immune-competent adult mice are resistant to ZIKV infection in part because ZIKV fails to
89 effectively antagonize Stat2-dependent IFN responses in mice despite ZIKV NS5 protein binds and
90 degrades STAT2 for the immune evasion. (30-33). Thus, we used adult type I IFN receptor IFNAR
91 knockout (*Ifnar1*^{-/-}) mice as a ZIKV infection mouse model to examine proinflammatory responses
92 in the CNS and the neuropathogenesis of ZIKV infection. RNA-seq analysis was performed to
93 examine neuroinflammation in response to ZIKV infection in the brains of *Ifnar1*^{-/-} mice. We
94 focused on the immune cells in the central nervous system that are susceptible to ZIKV infection and
95 consequently contribute to neuroinflammation in this animal model.

96

97 **Results**

98 **ZIKV infection of the brain induces proinflammatory responses in *Ifnar1*^{-/-} mice.**

99 When *Ifnar1*^{-/-} C57BL/6 mice were infected with 10³ plaque-forming units (PFU) of the
100 PRVABC59 strain of ZIKV via a subcutaneous route, most infected mice became paralyzed on at
101 least one hind limb at 9 days post infection (dpi) (Fig. 1A). To our knowledge, there are two

102 mechanisms underlying ZIKV-associated paralysis in *Ifnar1*^{-/-} mice. First, ZIKV infection of
103 astrocytes breaks down the blood-brain barrier of *Ifnar1*^{-/-} mice, leading to a large influx of CD8+ T
104 cells that promotes paralysis (34). Second, ZIKV infection in the spinal cord of *Ifnar1*^{-/-} mice results
105 in motor neuron synaptic retraction and inflammation (35). To address whether infection in the brain
106 or spinal cord accounts for paralysis in ZIKV infected mice, we assessed the viral load at 6 dpi in the
107 brain and spinal cord along with that in the eyes, kidneys, testes, and ovaries, which are reported as
108 ZIKV susceptible organs (Fig. 1B). High levels of viral RNA were detected in both the brain and
109 spinal cord, but the levels in the spinal cord were higher than those in the brain. Next, we analyzed
110 the mRNA levels of proinflammatory cytokines, including IL-1 β , IL-6, IFN- γ , and TNF- α , in the
111 brain and spinal cord using RT-qPCR at 6 dpi (Fig. 1C). Notably, the mRNA expression of
112 proinflammatory cytokines in the brains of ZIKV-infected mice was much higher than that in the
113 spinal cord. Upregulated proinflammatory cytokine expression in the ZIKV-infected mouse brain
114 was confirmed using ELISA (Fig. 1D). These results indicated that ZIKV infection of the brain
115 induces proinflammatory responses that contribute to neuroinflammation.

116 **Distinct transcriptional signatures and gene expression changes in the brain of ZIKV-infected
117 *Ifnar1*^{-/-} mice.**

118 To assess the effects of ZIKV infection on gene expression in the mouse brain, we performed RNA-
119 seq on brain homogenates of ZIKV-infected *Ifnar1*^{-/-} mice at 0, 3, and 6 dpi. Genes with adjusted *P*-
120 value < 0.05 were considered differentially expressed genes (DEGs). We identified 930 DEGs at 6
121 dpi (Up-regulated: 546; Down-regulated: 384) that were differentially expressed compared to those
122 at 0 dpi whereas there were 56 DEGs at 3 dpi (Up-regulated: 19; Down-regulated: 37). The volcano
123 plot for DEGs at 6 dpi versus 0 dpi showed that several highly significant DEGs associated with IFN
124 signaling were upregulated (Fig. 2A). According to the enrichment analysis of the biological
125 category of gene ontology (GO), DEGs at 6 dpi were highly enriched in the cytokine-mediated
126 signaling pathway, inflammatory responses, neutrophil-mediated immunity (Fig. 2B). The

127 upregulation of DEGs involved in the immune response was most conspicuous at 6 dpi (Fig. 2C).
128 Particularly, genes of proinflammatory cytokines (Il1b, Il6, and Tnf) and complement components
129 (C1qa, C3, and C4b) in the inflammatory response were upregulated at 6 dpi (Fig. 2D). In addition,
130 genes in the IFN signaling pathway (Oas1a, Oas2, Stat1, Stat2, Irf1, and Irf7) were upregulated at 6
131 dpi (Fig. 2E). Collectively, RNA-seq data from the brains of ZIKV-infected mice showed distinct
132 immune and inflammatory signatures at 6 dpi.

133 **ZIKV infection results in infiltration and proinflammatory activation of macrophages but not**
134 **microglia in the *Ifnar1*^{-/-} mouse brain.**

135 To identify the immune cells in the brain that are responsible for the proinflammatory responses to
136 ZIKV infection, we isolated the mouse brain after ZIKV infection. The brain homogenates were used
137 to isolate immune cells in the brain, including microglia, macrophages, and lymphocytes, by 30 %
138 and 70 % Percoll gradient centrifugation, followed by flow cytometry analysis of cell surface
139 markers such as CD11b and CD45, as illustrated in Fig. 3A. The isolate consisted of three
140 populations, namely lymphocytes (CD11b⁻ and CD45^{High}), macrophages (CD11b⁺ and CD45^{High}), and
141 microglia (CD11b⁺ and CD45^{Low}), and their population was altered by ZIKV infection (Fig. 3B).
142 While the number of microglia or lymphocytes in the brain did not change, that of macrophages
143 increased approximately four-fold in response to ZIKV infection, possibly indicating macrophage
144 brain infiltration (Fig. 3C–E). This pattern of alteration by ZIKV infection was different from that
145 obtained by SARS-CoV-2 infection in our previous study, in which microglia were significantly
146 depopulated (36). Next, we analyzed the IL-1 β , IL-6, and TNF- α responses in each of the three
147 populations (Fig. 4A). Interestingly, only the numbers of IL-1 β -positive macrophages and
148 lymphocytes, but not those of microglia, dramatically increased (Fig. 4B–F). These results suggest a
149 role for macrophages and lymphocytes in IL-1 β -mediated inflammation in the brains of ZIKV-
150 infected mice.

151 We then investigated whether IL-1 β expression in macrophages and lymphocytes was mediated by
152 direct ZIKV infection. To address this, we used an anti-flavivirus envelope protein antibody (4G2) to
153 stain ZIKV-infected cells along with IL-1 β in the three isolated populations (Fig. 5A). As previous
154 studies have demonstrated that microglia and macrophages are susceptible to ZIKV infection (18,
155 37-39), we observed that they were infected with ZIKV whereas lymphocytes were not infected (Fig.
156 5B-D). While ZIKV infection of microglia in *Ifnar1*^{-/-} mice did not lead to microglial activation
157 (Fig. 4B, 5E), infection of macrophages resulted in the induction of IL-1 β (Fig. 4C, 5F).
158 Lymphocytes showed elevated IL-1 β levels, but they were not infected with ZIKV (Fig. 4D, 5G).
159 These findings demonstrate that IL-1 β induction in the brains of ZIKV-infected *Ifnar1*^{-/-} mice was
160 likely due to ZIKV-infected macrophages and lymphocytes, but not microglia.

161 **ZIKV infection of THP-1 cells induces IL-1 β secretion and inflammatory cell death**

162 Next, we used human monocyte THP-1 cells to confirm our *in vivo* observations. Given the key role
163 of NLRP3 inflammasome in innate immune responses by activating caspase-1 to promote IL-1 β
164 secretion and pyroptosis (40), we examined whether ZIKV infection stimulates IL-1 β secretion
165 through NLRP3 inflammasome activation in THP-1 cells. When THP-1 cells were infected with
166 ZIKV at a multiplicity of infection (MOI) of 0.1, the viral RNA and envelope protein levels were
167 increased in a time-dependent manner, as shown by RT-qPCR and western blotting, respectively (Fig.
168 6A, 6B). ELISA revealed that, compared to the mock infection, ZIKV infection significantly
169 augmented IL-1 β secretion over time (Fig. 6C). In addition to the increase in IL-1 β secretion, cell
170 death was promoted by ZIKV infection in THP-1 cells, possibly due to pyroptosis (Fig. 6D).
171 Consequently, we determined whether caspase-1 and GSDMD cleavage resulting from activation of
172 the NLRP3 inflammasome were induced by ZIKV infection. Caspase-1 and Gasdermin D (GSDMD)
173 cleavage was observed from 1 dpi, followed by IL-1 β maturation and secretion (Fig. 6E). Thus,
174 ZIKV infection of THP-1 cells activates the NLRP3 inflammasome and consequently induces IL-1 β
175 maturation and secretion.

176 **The increase in C3 levels by ZIKV infection is mediated by IL-1 β signaling**

177 Previous studies have revealed that IL-1 β and other proinflammatory cytokines induce the
178 transcription factor CCAAT/enhancer binding protein β (C/EBP- β); this transcription factor directly
179 activates the promoter of C3, which plays a crucial role in the activation of the complement system
180 and contributes to innate immune responses (27, 41, 42). To validate the role of C/EBP- β in IL-1 β -
181 mediated induction of C3 expression by ZIKV infection in THP-1 cells, we infected cells with ZIKV
182 at 5 MOI and analyzed the activation of P38, Erk 1/2, and C/EBP- β using western blotting. Indeed,
183 ZIKV infection induced C/EBP- β expression and its activation through phosphorylation, which was
184 conducted by activated p38 but not Erk 1/2, resulting in the elevation of C3 expression (Fig. 7A). C3
185 induction was suppressed by C/EBP- β knockout in ZIKV-infected THP-1 cells (Fig. 7B). Diacerein,
186 an inhibitor of IL-1 β production (43), and an IL-1R antagonist effectively reduced the ZIKV-
187 mediated C3 induction in a dose-dependent manner, suggesting the involvement of IL-1 β in the
188 induction of C3 gene expression by ZIKV infection (Fig. 7C, 7D). The reduction of C3 secretion by
189 Diacerein and the IL-1R antagonist was confirmed by ELISA (Fig. 7E, 7F). Therefore, we
190 demonstrated that ZIKV infection in THP-1 cells promotes C/EBP- β expression through IL-1 β
191 induction, eventually leading to increased C3 levels.

192 In the brains of *Ifnar1*^{-/-} mice, the induction and activation of C/EBP- β by ZIKV infection were
193 determined at 6 dpi using RT-qPCR and western blot analysis (Fig. 8A, 8B). The increased
194 expression and activation of C/EBP- β led to the induction of C3 mRNA and protein expression as
195 determined by RT-qPCR and ELISA, respectively (Fig. 8C, 8D). We also detected C3 induction in
196 mouse sera following ZIKV infection, which indicated systemic C3 induction. To evaluate the
197 functional consequences of C3 induction and complement activation by ZIKV infection, we
198 determined the C5a levels in the brain. As expected, the C5a levels in the brains of ZIKV-infected
199 mice were significantly increased at 6 dpi (Fig. 8F). Taken together, our findings indicate that the
200 induction of C3 and complement activation by ZIKV infection is mediated by the IL-1 β signaling

201 pathway.

202

203 **Discussion**

204 To date, the neuropathogenesis of ZIKV infection remains unclear. Understanding the
205 neuropathogenesis of ZIKV infection would help to understand ZIKV-associated neurological
206 diseases. ZIKV infects human fetal brain microglia and macrophages (19). This induces high levels
207 of proinflammatory cytokines, which are implicated in ZIKV-derived neuroinflammation. C3 is
208 induced in most neurodegenerative diseases and is upregulated by proinflammatory cytokines such
209 as IL-1 β (24-27). Furthermore, IL-1 β and C3 expression is increased in different viral infections of
210 the CNS (28, 44). However, whether IL-1 β and C3 expression in the brain is affected by ZIKV
211 infection remains to be investigated. Here, we used adult *Ifnar1*^{-/-} mice as a ZIKV infection mouse
212 model to examine proinflammatory responses in the CNS upon ZIKV infection. We demonstrated
213 that ZIKV infection of the brain in this animal model augments IL-1 β expression in infiltrating
214 macrophages and elicits IL-1 β -mediated inflammation, leading to the destructive consequences of
215 neuroinflammation.

216 Neurons are targets in the CNS for ZIKV, JEV, and WNV infection (45-47). They are likely the first
217 responders to immune responses against neurotropic viral infections, producing type I IFNs and
218 expressing MHC class I molecules (48, 49). Upon initiation of an inflammatory response in the CNS,
219 proinflammatory cytokines are critical for recruitment of monocytes to the CNS (44). When we
220 infected the *Ifnar1*^{-/-} mice with ZIKV, increased pro-inflammatory cytokine levels and macrophage
221 infiltration were observed in the brain at 6 dpi (Fig. 1C, 1D, 3B, 3D). These results imply that ZIKV
222 infection can elicit neuronal inflammation and, consequently, monocyte infiltration in this animal
223 model.

224 Microglia and macrophages have been found to be of the same origin (50) and have similar functions,

225 such as production of inflammatory mediators (51). However, they play different roles in the brain.
226 Microglia may protect the injured brain, whereas macrophages concurrently damage the brain (52).
227 In this study, although both microglia and macrophages were infected with ZIKV at 6 dpi (Fig. 5B,
228 5E), macrophages showed proinflammatory activation with upregulated IL-1 β expression, but
229 microglia were not observed in the brains of infected *Ifnar1*^{-/-} mice (Fig. 4B, 4C, 5E, 5F).
230 Proinflammatory activated macrophages can accelerate the number of circulating immune cells and
231 increase their infiltration into the brain, also playing critical roles in pathophysiological processes.
232 Further studies are warranted to determine why ZIKV-infected microglia were not activated in the
233 brains of *Ifnar1*^{-/-} mice.
234 In ZIKV-GBS, particularly the acute inflammatory demyelinating polyneuropathy variant, cytokine-
235 mediated inflammation and macrophage activation may lead to peripheral nerve injury, and
236 complement activation may be associated with demyelinating neuropathies (8, 53). Given that IL-1
237 signaling is considered the upper hierarchical cytokine signaling cascade in the CNS (29), ZIKV
238 infection of the brain in *Ifnar1*^{-/-} mice induces IL-1 β expression in infiltrating macrophages (Fig. 3D,
239 4C, 5F) and elicits IL-1 β -mediated inflammation and macrophage activation, which can be
240 associated with the destructive consequences of neuroinflammation, such as peripheral neuropathy.
241 Our findings also suggest that ZIKV-induced IL-1 β secretion might lead to the expansion of
242 encephalitogenic T cells (54) and pyroptosis in CNS peripheral myeloid and lymphoid cells; these
243 cells can mediate neuroinflammation in multiple CNS diseases (55).
244 Complement is thought to have a protective effect, but exaggerated or insufficient activation of the
245 complement system can cause neuropathies and contribute to neurodegeneration and
246 neuroinflammation (24, 56). ZIKV infection upregulated C3 expression through IL-1 β -mediated
247 signaling (Fig. 7 and 8), possibly disrupting the balance of the complement system, which can
248 mediate myelin phagocytosis by macrophages (56). The anaphylatoxins (C3a, C4a, and C5a)
249 produced during complement activation play a major role in the pathogenesis of inflammatory

250 disorders, including ischemia/reperfusion injury, and are involved in various neurodegenerative
251 disorders (57). An increase in C5a in the cerebrospinal fluid was also detected during the
252 exacerbation of neuromyelitis (58). In this study, we observed an increase in C5a levels in the brains
253 of ZIKV-infected *Ifnar1*^{-/-} mice (Fig. 8F), suggesting its contribution to peripheral neuropathies (59).
254 In summary, ZIKV infection of the brain induced the expression of proinflammatory cytokines,
255 including IL-1 β , IL-6, IFN- γ , and TNF- α , in *Ifnar1*^{-/-} mice. RNA-seq analysis revealed that the
256 expression of genes involved in immune responses to viral infection and inflammatory responses in
257 the brains of these mice was significantly upregulated by ZIKV infection. Notably, infiltration and
258 pro-inflammatory activation of macrophages, but not microglia, were observed at 6 dpi in the ZIKV-
259 infected *Ifnar1*^{-/-} mice. ZIKV infection of THP-1 cells induced pyroptosis, increased IL-1 β release,
260 and consequently increased C3 expression. Increases in C3 and C5a levels in the brains of infected
261 mice were confirmed. Overall, our data suggest that ZIKV infection of the brains of *Ifnar1*^{-/-} mice
262 augments IL-1 β expression in infiltrating macrophages and elicits IL-1 β -mediated inflammation
263 through macrophage activation, which can be associated with the destructive consequences of
264 neuroinflammation.

265

266 **Materials and methods**

267 **Cells, plasmids, and virus**

268 THP-1 (TIB-202), a human leukemia monocytic cell line, and the ZIKV PRVABC59 strain (VR-
269 1843; GenBank [KU501215](#)) were purchased from the American Type Culture Collection (ATCC;
270 Manassas, VA, USA). This cell line was maintained in RPMI-1640 medium (Cytiva, Marlborough,
271 MA, USA) containing 10 % fetal bovine serum (FBS) (Gibco, Waltham, MA, USA) and 1 %
272 penicillin/streptomycin (Gibco). This virus was propagated in Vero cells (CCL-81; ATCC). Virus
273 titers were determined using plaque assay as described previously (60).

274 For CRISPR/Cas9-mediated knockout of C/EBP- β , we constructed CRISPR/Cas9 plasmids using the
275 LentiCRISPRv2-puro vector (Addgene #98290) (61, 62). LentiCRISPRv2-C/EBP- β plasmids were
276 generated by inserting hybridized oligonucleotides (#1:5'-CTCTTCTCCGACGACTACGG-3' and
277 5'-CCGTAGTCGTCGGAGGAGAG-3'; #2:5'-GGCCAACCTCTACTACGAGG-3' and 5'-
278 CCTCGTAGTAGAAGTTGGCC-3') into the BsmBI restriction sites. Lentivirus was produced from
279 70–80 % confluent HEK293T cells transfected with 0.2 μ g lentiviral plasmid, 0.5 μ g pVSV-G
280 (Addgene #8454), and 2.3 μ g psPAX2 (Addgene #12260) using 6 μ l of lipofectamine 2000
281 (Invitrogen). The lentiviral supernatant was harvested 48 h later and used for the transduction of
282 THP-1 cells by spinoculation. After 48 h post transduction, the cells were selected with 1 μ g/ml
283 puromycin (Gibco) for a further seven days.

284 **Drug treatment and cell viability assay**

285 Cells (1×10^6 cells per well) were plated into six-well plates and inoculated with 0.1 or 5 MOI ZIKV
286 in RPMI-1640 medium the next day. After 1 h incubation, cells were treated with Diacerein (D9302;
287 Sigma-Aldrich, St. Louis, MO, USA) or IL-1RA (SRP3327, Sigma-Aldrich). At the indicated time
288 points, the cells were washed with PBS by cell pelleting for cell lysates and RNA extraction. The
289 cells were lysed in radioimmunoprecipitation (RIPA) buffer (Thermo Fisher Scientific, Waltham,
290 MA, USA). Total cellular RNA was extracted using an RNeasy Mini Kit (QIAGEN, Hilden,
291 Germany). To determine cell viability, cells were monitored using Trypan Blue dye exclusion.

292 **Mice**

293 *Ifnar1*^{-/-} mice were purchased from B&K Universal Ltd. (Hull, UK). Mice were bred and housed in
294 a BSL-2 animal facility at the Korea Research Institute of Chemical Technology (KRICT). Male and
295 female mice were between six and eight weeks of age at the initiation of all the experiments. All
296 protocols were approved by the Institutional Animal Care and Use Committee (Protocol ID 8A-M6,
297 IACUC ID 2021-8A-02-01, and 2021-8A-03-03). Viral inoculations (10^3 pfu) were performed

298 subcutaneously under anesthesia using isoflurane in the BSL-2 animal facility, and all efforts were
299 made to minimize animal suffering. Body weight was measured daily post-infection. Neurological
300 symptoms were scored from 0 to 5 as follows: 0, no symptoms; 1, hindlimb weakness; 2, partial
301 hindlimb paralysis; 3, paralysis of one hindlimb; 4, paralysis of both hindlimbs; and 5, moribund or
302 dead.

303 **Mononuclear cell isolation**

304 Mononuclear cells isolation in the mouse brain was performed following the protocols as previously
305 described (36, 63, 64). Mock- or ZIKV-infected mice were anesthetized with isoflurane, followed by
306 perfusion with 10 ml of cold 1× DPBS (Gibco) into the left ventricle to remove blood from the
307 tissues. The brains were transferred to a six-well plate containing cold Hanks' balanced salt solution
308 (HBSS) (Gibco), and the plates were kept on ice. The generation of brain cell suspensions by a 70
309 μ m pore sized-cell strainer (SPL, Gyeonggi-do, South Korea) was made in 10 ml per brain of
310 digestion cocktail containing 0.5 mg/ml DNase I (Roche, Basel, Switzerland) and 1 mg/ml
311 Collagenase A (Roche) in HBSS. The suspension was incubated at room temperature for 30 min,
312 followed by centrifugation for 7 min at $300 \times g$ and 18 °C. The cell pellet was resuspended in 30 %
313 Percoll (Sigma-Aldrich) in HBSS and then slowly layered over 70 % Percoll in HBSS in a 15 ml
314 conical tube. Approximately 2 ml of the interphase volume was collected into a new tube after
315 gradient centrifugation for 40 min at $200 \times g$ at 18 °C. Isolated mononuclear cells were washed three
316 more times in a volume of 500 μ L of HBSS containing 0.01 M HEPES (Gibco), using a
317 microcentrifuge for 7 min at $600 \times g$ at 4 °C.

318 **Flow cytometry analysis**

319 Isolated brain mononuclear cells from the mock or ZIKV-infected mice in cell staining buffer (PBS
320 with 1 % FBS and 0.09 % NaN_3) were stained for 30 min with fluorescence-conjugated antibodies,
321 namely, Brilliant Violet 421 anti-mouse/human CD11b Antibody (101236, BioLegend, San Diego,

322 CA, USA), PE/Cyanine7 anti-mouse CD45 Antibody (103114, BioLegend), APC anti-mouse TNF- α
323 Antibody (506307, BioLegend), FITC anti-mouse IL-6 Monoclonal Antibody (MP5-20F3) (11-7061-
324 82, eBioscience, San Diego, CA, USA), PE anti-mouse IL-1 β Antibody (12-7114-82, eBioscience),
325 and Alexa Fluor 488 anti-flavivirus group antigen antibody (4G2) (NBP2-52709AF488, Novus
326 Biologicals, Englewood, CO, USA). The cells were then analyzed using a FACS Aria III sorter (BD
327 Biosciences, San Jose, CA, USA), and data were analyzed using FlowJo software (BD Biosciences).
328 All fluorochromes were compensated for.

329 **RT-qPCR**

330 Quantitative RT-PCR (QuantStudio 3, Applied Biosystems, Foster City, CA, USA) was performed
331 using one-step Prime script III RT-qPCR mix (Takara Bio, Shiga, Japan). The viral RNA of ZIKV
332 NS3 was detected by customized probe-based qPCR assay (Integrated DNA Technologies, Coralville,
333 IA, USA). The Il1b, Il6, Tnf, Ifng, Cebpb, and C3 genes were also detected using individual
334 customized probes (Integrated DNA Technologies). The sequences of the qPCR probes and primers
335 used in this study are listed in Table S1.

336 **RNA-seq and analysis**

337 The sequencing library was prepared using the TruSeq Stranded mRNA Sample Prep Kit and
338 sequenced on NovaSeq 6000 (Illumina, San Diego, CA, USA), yielding more than 6G bases of
339 sequence for each sample. Adaptor sequences were removed from the sequenced reads using
340 Cutadapt (version 3.1) (65) and aligned to the hybrid reference genomes of humans
341 (GRCh38.p13_ENS100) and ZIKV with the STAR aligner (version 2.7.6a) (66). Aligned reads were
342 quantified at the gene level by HTSeq (version 0.13.5) (67) with “intersection-nonempty” mode.
343 Genes with lower than five counts for the total count per gene were removed for further analysis.
344 Differentially expressed genes were analyzed with DESeq2 (version 1.30.1) (68) using abs(log2 fold
345 change) > 1 and adjusted P-value (Benjamini-Hochberg) < 0.01 as the cut-off. Multidimensional

346 scaling analysis was performed with the clustermap function in the Python seaborn package (version
347 0.11.1) using genes with a mean FPKM > 1 among the samples and transformed to log2(FPKM+1).
348 Over-representation analysis of the DEGs enriched in GO Biological Process 2018 was performed
349 with EnrichR (69) and an adjusted P-value (Benjamini-Hochberg) < 0.05.

350 **ELISA**

351 Culture supernatants collected from infected cells, brain homogenates, and mouse sera were used for
352 the detection of IL-1 β , IL-6, TNF- α , IFN- γ , C3, and C5a. The concentration of each of them was
353 determined using an ELISA kit ([human IL-1 β , K0331800; mouse IL-1 β , K0331231; IL-6,
354 K0331230; TNF- α , K0331186; IFN- γ , K0331138; Komabiotech, Seoul, Korea]; [mouse C3,
355 ab263884; C5a, ab193718; Abcam, Cambridge, UK]), according to the manufacturer's instructions.

356 **Western blotting**

357 Proteins in the lysate were separated on a denaturing polyacrylamide gel and transferred to a
358 polyvinylidene fluoride (PVDF) membrane (Merck Millipore, Burlington, MA, USA). The
359 membrane was incubated with 5 % skim milk (BD Biosciences) in Tris-buffered saline with 0.1 %
360 Tween 20 (TBST) buffer and the primary antibodies, namely, anti-IL-1 β (GTX130021, GeneTex,
361 Irvine, CA, USA), anti-GSDMDC1 (sc-81868, Santa Cruz Biotechnology), anti- β -actin (sc-47778,
362 Santa Cruz Biotechnology), anti-Caspase-1 (3866S, Cell Signaling Technology), anti-pan-flavivirus
363 E (4G2, purified in the lab), anti-C3 (ab200999, Abcam), anti-C/EBP- β (90081S, Cell Signaling
364 Technology), anti-C/EBP- β (LAP) (3087S, Cell Signaling Technology), anti-phospho-C/EBP- β
365 (Thr235) (3084S, Cell Signaling Technology), anti-p38 MAPK (9212S, Cell Signaling Technology),
366 anti-phospho-p38 MAPK (9211S, Cell Signaling Technology), anti-p44/42 MAPK (9102S, Cell
367 Signaling Technology), anti-phospho-p44/42 MAPK (4370S, Cell Signaling Technology).
368 Horseradish peroxidase (HRP)-conjugated secondary antibodies from Bio-Rad and enhanced
369 chemiluminescence (ECL) reagents (Thermo Fisher Scientific) were used for protein detection.

370 **Statistical analysis**

371 All experiments were performed at least thrice. All data were analyzed using the GraphPad Prism 8.0
372 software (GraphPad Software, San Diego, CA, USA). $P < 0.05$ was considered statistically
373 significant. Specific analysis methods are described in the figure legends.

374

375 **Acknowledgments**

376 This work was supported by the National Research Foundation of Korea (NRF) grant funded by the
377 Ministry of Education, Science, and Technology (MIST) of the Korean government
378 (2020R1C1C1003379) and the National Research Council of Science & Technology (NST) grant
379 funded by the Korean government (MSIP) (CRC-16-01-KRICT). The authors declare that they have
380 no conflicts of interest.

381 Conceptualization: G.U.J., S.L., and Y.-C.K.; methodology: G.U.J., S.L., and Y.-C.K.; investigation:
382 G.U.J., S.L., D.Y.K., J.K., G.Y.Y., and J.K.; writing: G.U.J. and Y.-C.K.; review and editing: G.U.J.,
383 S.L., and Y.-C.K.; funding acquisition: Y.-C.K.; and supervision: Y.-C.K.

384 The authors declare that they have no conflicts of interest.

385

386 **References**

- 387 1. Ikejezie J, Shapiro CN, Kim J, Chiu M, Almiron M, Ugarte C, et al. Zika virus transmission—region
388 of the Americas, May 15, 2015–December 15, 2016. Morbidity and Mortality Weekly Report.
389 2017;66(12):329.
- 390 2. de Araújo TVB, Rodrigues LC, de Alencar Ximenes RA, de Barros Miranda-Filho D, Montarroyos
391 UR, de Melo APL, et al. Association between Zika virus infection and microcephaly in Brazil, January to
392 May, 2016: preliminary report of a case-control study. The lancet infectious diseases. 2016;16(12):1356-63.
- 393 3. Mattar S, Ojeda C, Arboleda J, Arrieta G, Bosch I, Botia I, et al. Case report: microcephaly
394 associated with Zika virus infection, Colombia. BMC infectious diseases. 2017;17(1):1-4.
- 395 4. Cao-Lormeau V-M, Blake A, Mons S, Lastère S, Roche C, Vanhomwegen J, et al. Guillain-Barré

396 Syndrome outbreak associated with Zika virus infection in French Polynesia: a case-control study. The
397 Lancet. 2016;387(10027):1531-9.

398 5. Mécharles S, Herrmann C, Poullain P, Tran T-H, Deschamps N, Mathon G, et al. Acute myelitis due
399 to Zika virus infection. The Lancet. 2016;387(10026):1481.

400 6. Carteaux G, Maquart M, Bedet A, Contou D, Brugières P, Fourati S, et al. Zika virus associated with
401 meningoencephalitis. New England Journal of Medicine. 2016;374(16):1595-6.

402 7. Soares CN, Brasil P, Carrera RM, Sequeira P, De Filippis AB, Borges VA, et al. Fatal encephalitis
403 associated with Zika virus infection in an adult. Journal of Clinical Virology. 2016;83:63-5.

404 8. Muñoz LS, Parra B, Pardo CA, Study NEitA. Neurological implications of Zika virus infection in
405 adults. The Journal of infectious diseases. 2017;216(suppl_10):S897-S905.

406 9. Platt DJ, Smith AM, Arora N, Diamond MS, Coyne CB, Miner JJ. Zika virus-related neurotropic
407 flaviviruses infect human placental explants and cause fetal demise in mice. Science translational medicine.
408 2018;10(426):eaao7090.

409 10. Da Silva IRF, Frontera JA, De Filippis AMB, Do Nascimento OJM, Group R-G-ZR. Neurologic
410 complications associated with the Zika virus in Brazilian adults. JAMA neurology. 2017;74(10):1190-8.

411 11. Rozé B, Najioullah F, Fergé J-L, Apetse K, Brouste Y, Cesaire R, et al. Zika virus detection in urine
412 from patients with Guillain-Barre syndrome on Martinique, January 2016. Eurosurveillance.
413 2016;21(9):30154.

414 12. Azevedo RS, Araujo MT, Martins Filho AJ, Oliveira CS, Nunes BT, Cruz AC, et al. Zika virus
415 epidemic in Brazil. I. Fatal disease in adults: clinical and laboratorial aspects. Journal of Clinical Virology.
416 2016;85:56-64.

417 13. Alves-Leon SV, Lima MdR, Nunes PCG, Chimelli LMC, Rabelo K, Nogueira RMR, et al. Zika virus
418 found in brain tissue of a multiple sclerosis patient undergoing an acute disseminated encephalomyelitis-
419 like episode. Multiple Sclerosis Journal. 2019;25(3):427-30.

420 14. Tang H, Hammack C, Ogden SC, Wen Z, Qian X, Li Y, et al. Zika virus infects human cortical
421 neural progenitors and attenuates their growth. Cell stem cell. 2016;18(5):587-90.

422 15. Devhare P, Meyer K, Steele R, Ray RB, Ray R. Zika virus infection dysregulates human neural stem
423 cell growth and inhibits differentiation into neuroprogenitor cells. Cell death & disease. 2017;8(10):e3106-e.

424 16. Li C, Xu D, Ye Q, Hong S, Jiang Y, Liu X, et al. Zika virus disrupts neural progenitor development
425 and leads to microcephaly in mice. Cell stem cell. 2016;19(1):120-6.

426 17. Quicke KM, Bowen JR, Johnson EL, McDonald CE, Ma H, O'Neal JT, et al. Zika virus infects human
427 placental macrophages. Cell host & microbe. 2016;20(1):83-90.

428 18. Meertens L, Labeau A, Dejarnac O, Cipriani S, Sinigaglia L, Bonnet-Madin L, et al. Axl mediates
429 ZIKA virus entry in human glial cells and modulates innate immune responses. Cell reports.
430 2017;18(2):324-33.

431 19. Lum F-M, Low DK, Fan Y, Tan JJ, Lee B, Chan JK, et al. Zika virus infects human fetal brain
432 microglia and induces inflammation. Clinical Infectious Diseases. 2017;64(7):914-20.

433 20. Cervellati C, Trentini A, Pecorelli A, Valacchi G. Inflammation in neurological disorders: the thin
434 boundary between brain and periphery. Antioxidants & Redox Signaling. 2020;33(3):191-210.

435 21. Simi A, Tsakiri N, Wang P, Rothwell N. Interleukin-1 and inflammatory neurodegeneration.

436 Biochemical Society Transactions. 2007;35(5):1122-6.

437 22. Zhao M-L, Kim M-O, Morgello S, Lee SC. Expression of inducible nitric oxide synthase, interleukin-1 and caspase-1 in HIV-1 encephalitis. Journal of neuroimmunology. 2001;115(1-2):182-91.

438 23. Xing HQ, Hayakawa H, Izumo K, Kubota R, Gelpi E, Budka H, et al. In vivo expression of proinflammatory cytokines in HIV encephalitis: an analysis of 11 autopsy cases. Neuropathology. 2009;29(4):433-42.

439 24. Bonifati DM, Kishore U. Role of complement in neurodegeneration and neuroinflammation. Molecular immunology. 2007;44(5):999-1010.

440 25. Barnum SR, Jones JL, Benveniste EN. Interferon-gamma regulation of C3 gene expression in human astrogloma cells. Journal of neuroimmunology. 1992;38(3):275-82.

441 26. Barnum SR, Jones JL, Benveniste EN. Interleukin-1 and tumor necrosis factor-mediated regulation of C3 gene expression in human astrogloma cells. Glia. 1993;7(3):225-36.

442 27. Cardinaux JR, Allaman I, Magistretti PJ. Pro-inflammatory cytokines induce the transcription factors C/EBP β and C/EBP δ in astrocytes. Glia. 2000;29(1):91-7.

443 28. Speth C, Williams K, Hagleitner M, Westmoreland S, Rambach G, Mohsenipour I, et al. Complement synthesis and activation in the brain of SIV-infected monkeys. Journal of neuroimmunology. 2004;151(1-2):45-54.

444 29. Basu A, Krady JK, Levison SW. Interleukin-1: a master regulator of neuroinflammation. Journal of neuroscience research. 2004;78(2):151-6.

445 30. Grant A, Ponia SS, Tripathi S, Balasubramaniam V, Miorin L, Sourisseau M, et al. Zika virus targets human STAT2 to inhibit type I interferon signaling. Cell host & microbe. 2016;19(6):882-90.

446 31. Kumar A, Hou S, Airo AM, Limonta D, Mancinelli V, Branton W, et al. Zika virus inhibits type-I interferon production and downstream signaling. EMBO reports. 2016;17(12):1766-75.

447 32. Lazear HM, Govero J, Smith AM, Platt DJ, Fernandez E, Miner JJ, et al. A mouse model of Zika virus pathogenesis. Cell host & microbe. 2016;19(5):720-30.

448 33. Bowen JR, Quicke KM, Maddur MS, O'Neal JT, McDonald CE, Fedorova NB, et al. Zika virus antagonizes type I interferon responses during infection of human dendritic cells. PLoS pathogens. 2017;13(2):e1006164.

449 34. Jurado KA, Yockey LJ, Wong PW, Lee S, Huttner AJ, Iwasaki A. Antiviral CD8 T cells induce Zika-virus-associated paralysis in mice. Nature microbiology. 2018;3(2):141-7.

450 35. Morrey JD, Oliveira AL, Wang H, Zukor K, de Castro MV, Siddharthan V. Zika virus infection causes temporary paralysis in adult mice with motor neuron synaptic retraction and evidence for proximal peripheral neuropathy. Scientific reports. 2019;9(1):1-15.

451 36. Jeong GU, Lyu J, Kim K-D, Chung YC, Yoon GY, Lee S, et al. SARS-CoV-2 Infection of Microglia Elicits Proinflammatory Activation and Apoptotic Cell Death. Microbiology Spectrum. 2022:e01091-22.

452 37. Xu P, Shan C, Dunn TJ, Xie X, Xia H, Gao J, et al. Role of microglia in the dissemination of Zika virus from mother to fetal brain. PLoS neglected tropical diseases. 2020;14(7):e0008413.

453 38. Richard AS, Shim B-S, Kwon Y-C, Zhang R, Otsuka Y, Schmitt K, et al. AXL-dependent infection of human fetal endothelial cells distinguishes Zika virus from other pathogenic flaviviruses. Proceedings of the National Academy of Sciences. 2017;114(8):2024-9.

476 39. Yang D, Chu H, Lu G, Shuai H, Wang Y, Hou Y, et al. STAT2-dependent restriction of Zika virus by
477 human macrophages but not dendritic cells. *Emerging microbes & infections*. 2021;10(1):1024-37.

478 40. Faria SS, Costantini S, de Lima VCC, de Andrade VP, Rialland M, Cedric R, et al. NLRP3
479 inflammasome-mediated cytokine production and pyroptosis cell death in breast cancer. *Journal of*
480 *Biomedical Science*. 2021;28(1):1-15.

481 41. Hernandez-Encinas E, Aguilar-Morante D, Cortes-Canteli M, Morales-Garcia JA, Gine E, Santos A,
482 et al. CCAAT/enhancer binding protein β directly regulates the expression of the complement component
483 3 gene in neural cells: implications for the pro-inflammatory effects of this transcription factor. *Journal of*
484 *neuroinflammation*. 2015;12(1):1-16.

485 42. Mazumdar B, Kim H, Meyer K, Bose SK, Di Bisceglie AM, Ray RB, et al. Hepatitis C virus proteins
486 inhibit C3 complement production. *Journal of virology*. 2012;86(4):2221-8.

487 43. Yaron M, Shirazl I, Yaron I. eAnti-interleukin-1 effects of diacerein and rhein in human
488 osteoarthritic synovial tissue and cartilage cultures. *Osteoarthritis and Cartilage*. 1999;7(3):272-80.

489 44. Klein RS, Garber C, Funk KE, Salimi H, Soung A, Kanmogne M, et al. Neuroinflammation during
490 RNA viral infections. *Annual review of immunology*. 2019;37:73.

491 45. Figueiredo CP, Barros-Aragão FG, Neris RL, Frost PS, Soares C, Souza IN, et al. Zika virus replicates
492 in adult human brain tissue and impairs synapses and memory in mice. *Nature communications*.
493 2019;10(1):1-16.

494 46. Kalia M, Khasa R, Sharma M, Nain M, Vrati S. Japanese encephalitis virus infects neuronal cells
495 through a clathrin-independent endocytic mechanism. *Journal of virology*. 2013;87(1):148-62.

496 47. Klein RS, Lin E, Zhang B, Luster AD, Tollett J, Samuel MA, et al. Neuronal CXCL10 directs CD8+ T-
497 cell recruitment and control of West Nile virus encephalitis. *Journal of virology*. 2005;79(17):11457-66.

498 48. Delhaye S, Paul S, Blakqori G, Minet M, Weber F, Staeheli P, et al. Neurons produce type I
499 interferon during viral encephalitis. *Proceedings of the National Academy of Sciences*. 2006;103(20):7835-
500 40.

501 49. Chevalier G, Suberbielle E, Monnet C, Duplan V, Martin-Blondel G, Farrugia F, et al. Neurons are
502 MHC class I-dependent targets for CD8 T cells upon neurotropic viral infection. *PLoS pathogens*.
503 2011;7(11):e1002393.

504 50. Ginhoux F, Greter M, Leboeuf M, Nandi S, See P, Gokhan S, et al. Fate mapping analysis reveals
505 that adult microglia derive from primitive macrophages. *Science*. 2010;330(6005):841-5.

506 51. Xiong X-Y, Liu L, Yang Q-W. Functions and mechanisms of microglia/macrophages in
507 neuroinflammation and neurogenesis after stroke. *Progress in neurobiology*. 2016;142:23-44.

508 52. Yamasaki R, Lu H, Butovsky O, Ohno N, Rietsch AM, Cialic R, et al. Differential roles of microglia
509 and monocytes in the inflamed central nervous system. *Journal of Experimental Medicine*.
510 2014;211(8):1533-49.

511 53. Hafer-Macko C, Sheikh K, Li C, Ho T, Cornblath D, McKhann G, et al. Immune attack on the
512 Schwann cell surface in acute inflammatory demyelinating polyneuropathy. *Annals of Neurology: Official*
513 *Journal of the American Neurological Association and the Child Neurology Society*. 1996;39(5):625-35.

514 54. Dinarello CA. Interleukin-1 in the pathogenesis and treatment of inflammatory diseases. *Blood*,
515 *The Journal of the American Society of Hematology*. 2011;117(14):3720-32.

516 55. McKenzie BA, Dixit VM, Power C. Fiery cell death: pyroptosis in the central nervous system.
517 Trends in neurosciences. 2020;43(1):55-73.

518 56. Ramaglia V, Daha M, Baas F. The complement system in the peripheral nerve: friend or foe?
519 Molecular immunology. 2008;45(15):3865-77.

520 57. Guo R-F, Ward PA. Role of C5a in inflammatory responses. Annu Rev Immunol. 2005;23:821-52.

521 58. Kuroda H, Fujihara K, Takano R, Takai Y, Takahashi T, Misu T, et al. Increase of complement
522 fragment C5a in cerebrospinal fluid during exacerbation of neuromyelitis optica. Journal of
523 neuroimmunology. 2013;254(1-2):178-82.

524 59. Giorgio C, Zippoli M, Cocchiaro P, Castelli V, Varrassi G, Aramini A, et al. Emerging role of C5
525 complement pathway in peripheral neuropathies: Current treatments and future perspectives.
526 Biomedicines. 2021;9(4):399.

527 60. Shim B-S, Kwon Y-C, Ricciardi MJ, Stone M, Otsuka Y, Berri F, et al. Zika virus-immune plasmas
528 from symptomatic and asymptomatic individuals enhance Zika pathogenesis in adult and pregnant mice.
529 MBio. 2019;10(4):e00758-19.

530 61. Sanjana NE, Shalem O, Zhang F. Improved vectors and genome-wide libraries for CRISPR
531 screening. Nature methods. 2014;11(8):783-4.

532 62. Stringer BW, Day BW, D'Souza RC, Jamieson PR, Ensley KS, Bruce ZC, et al. A reference collection
533 of patient-derived cell line and xenograft models of proneural, classical and mesenchymal glioblastoma.
534 Scientific reports. 2019;9(1):1-14.

535 63. Cardona AE, Huang D, Sasse ME, Ransohoff RM. Isolation of murine microglial cells for RNA
536 analysis or flow cytometry. Nature protocols. 2006;1(4):1947-51.

537 64. Garcia JA, Cardona SM, Cardona AE. Isolation and analysis of mouse microglial cells. Current
538 protocols in immunology. 2014;104(1):14.35. 1-14.35. 15.

539 65. Martin M. Cutadapt removes adapter sequences from high-throughput sequencing reads. EMBnet
540 journal. 2011;17(1):10-2.

541 66. Dobin A, Davis CA, Schlesinger F, Drenkow J, Zaleski C, Jha S, et al. STAR: ultrafast universal RNA-
542 seq aligner. Bioinformatics. 2013;29(1):15-21.

543 67. Anders S, Pyl PT, Huber W. HTSeq—a Python framework to work with high-throughput
544 sequencing data. bioinformatics. 2015;31(2):166-9.

545 68. Love MI, Huber W, Anders S. Moderated estimation of fold change and dispersion for RNA-seq
546 data with DESeq2. Genome biology. 2014;15(12):1-21.

547 69. Kuleshov MV, Jones MR, Rouillard AD, Fernandez NF, Duan Q, Wang Z, et al. Enrichr: a
548 comprehensive gene set enrichment analysis web server 2016 update. Nucleic acids research.
549 2016;44(W1):W90-W7.

550

551 **Figure legends**

552 **Fig. 1** ZIKV infection of the brain elicits pro-inflammatory responses in *Ifnar1*^{-/-} mice. (A) *Ifnar1*^{-/-}

553 mice were subcutaneously infected with 10^3 PFU of ZIKV or PBS (mock). They were monitored
554 daily for neurological disease score as described in Materials and Methods. (B) Viral RNA levels in
555 the brain, spinal cord, eyes, kidney, testes, and ovary were assessed using RT-qPCR at 6 dpi. (C)
556 RNA extracted from the brain and spinal cord homogenates was used to assess mRNA levels of
557 proinflammatory cytokines, including IL-1 β , IL-6, IFN- γ , and TNF- α , by RT-qPCR at 6 dpi. (D) The
558 brain homogenates were used to measure protein levels of proinflammatory cytokines by ELSIA at 6
559 dpi. Statistically significant differences between the groups were determined using multiple two-
560 tailed t-tests (A), one-way analysis of variance (ANOVA; B), and Student's t-test (C, D); * $P < 0.05$;
561 ** $P < 0.01$; *** $P < 0.001$; **** $P < 0.0001$. Bars indicate mean \pm SEM.

562 **Fig. 2** RNA-seq analysis of the brain in ZIKV-infected mice. *Ifnar1*^{-/-} mice were infected with 10^3
563 PFU of ZIKV (n = 4 per indicated dpi). RNA extracted from the brain homogenates was used for
564 RNA-seq analysis. (A) A volcano plot comparing DEGs from samples taken at 6 dpi versus 0 dpi. (B)
565 GO enrichment analysis of biological process terms enriched in upregulated genes from comparisons
566 of mice at 6 dpi versus 0 dpi. Terms were ranked by adjusted P value. (C–E) Heat maps of DEGs
567 during ZIKV infection enriched in (C) immune response, (D) inflammatory response, and (E)
568 cytokine-mediated signaling, identified through GO analysis. Gene expression levels in the heat
569 maps are z score–normalized values determined from $\log_2[CPM]$ values. NS: not significant; FC:
570 fold change;

571 **Fig. 3** Macrophage infiltration into the brain of ZIKV-infected mice. (A) Schematic of the
572 experiment for B to E, created with BioRender.com. *Ifnar1*^{-/-} mice were infected with 10^3 PFU of
573 ZIKV (n = 4) or PBS (mock; n = 4). At 6 dpi, brains of mock or ZIKV-infected mice were extracted
574 and used for Percoll gradient centrifugation to isolate mononuclear cells for the flow cytometry
575 analysis. The cellular surface of isolated mononuclear cells was stained with CD11b and CD45
576 antibodies. (B) Representative flow plot gated on leukocytes shows gating for microglia (MI,
577 CD11b $^+$, CD45 $^{\text{Low}}$), macrophages (M ϕ , CD11b $^+$, CD45 $^{\text{High}}$), and lymphocytes (Lym, CD11b $^-$,

578 CD45^{High}). (C–E) Bar graphs show the number of microglia (C), macrophages (D), and lymphocytes
579 (E) isolated per brain at 6 dpi. Statistically significant differences between the groups were
580 determined using Student's t-test (C–E); ns, not significant; ** $P < 0.01$; Bars indicate mean \pm SEM.

581 **Fig. 4** Proinflammatory activation of macrophages and lymphocytes by ZIKV infection in the mouse
582 brain. (A) Representative flow plots gated on microglia (upper), macrophages (middle), and
583 lymphocytes (lower) to show expression levels of proinflammatory cytokines, including IL-1 β , IL-6,
584 and TNF- α . (B–D) Bar graphs indicate the percentage of activated microglia (B), macrophages (C),
585 and lymphocytes (D) expressing IL-1 β , IL-6, and TNF- α . Statistically significant differences
586 between the groups were determined using Student's t-test (B–D); ns, not significant; ** $P < 0.01$;
587 **** $P < 0.0001$. Bars indicate mean \pm SEM.

588 **Fig. 5** Microglia and macrophage infection by ZIKV in the mouse brain. *Ifnar1*^{–/–} mice were
589 infected with 10³ PFU of ZIKV (n = 4) or PBS (Mock; n = 4). At 6 dpi, isolated mononuclear cells in
590 brains of mock or ZIKV-infected mice were used for the flow cytometry analysis. (A) Representative
591 flow plots gated on microglia (upper), macrophages (middle), and lymphocytes (lower) to show
592 expression levels of ZIKV envelop protein and IL-1 β . (B–D) Bar graphs indicate median
593 fluorescence intensities of ZIKV envelop protein-positive microglia (B), macrophages (C), and
594 lymphocytes (D). (E–G) Bar graphs indicate the percentage of activated microglia (E), macrophages
595 (F), and lymphocytes (G) expressing IL-1 β . Statistically significant differences between the groups
596 were determined using Student's t-test (B–G); ns, not significant; * $P < 0.05$; **** $P < 0.0001$. Bars
597 indicate mean \pm SEM.

598 **Fig. 6** ZIKV infection induces IL-1 β secretion and inflammatory cell death in THP-1 cells. THP-1
599 cells were infected with ZIKV at 0.1 MOI. (A) Viral loads in ZIKV-infected THP-1 cells were
600 determined by RT-qPCR at 0, 1, 2, and 3 dpi. (B) ZIKV envelop protein in cell lysates were
601 determined by western blot. Actin served as the loading control. (C) IL-1 β levels in the cell culture

602 media were measured by ELISA at 1, 2, and 3 dpi. (D) Dead cells were analyzed using Trypan Blue
603 dye exclusion at 1, 2, and 3 dpi. (E) Pro-caspase-1, cleaved caspase-1, GSDMD, cleaved GSDMD,
604 pro-IL-1 β , and mature IL-1 β in cell lysates or in supernatants were determined by western blot. Actin
605 served as the loading control. Statistically significant differences between the groups were
606 determined using one-way analysis of variance (ANOVA; A) and Student's t-test (C and D); *P <
607 0.05; **P < 0.01; ***P < 0.001. Bars indicate mean \pm SEM.

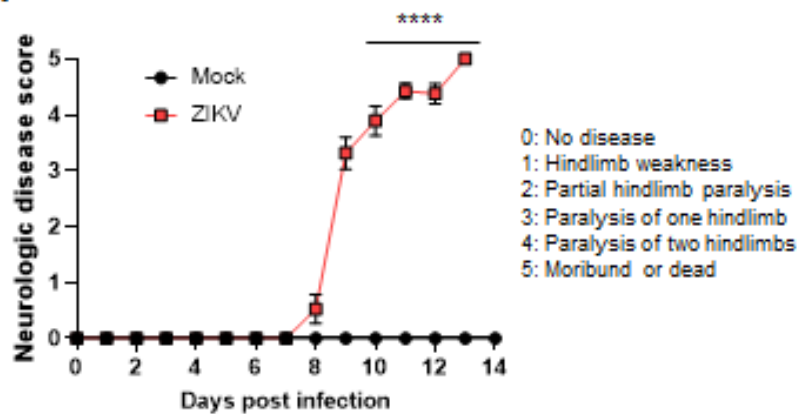
608 **Fig. 7** ZIKV infection induces C3 expression through IL-1 β signaling in THP-1 cells. (A) THP-1
609 cells were infected with ZIKV at 5 MOI or treated with 10 ng/ml IL-1 β . At 2 dpi, C3, phospho-p38,
610 p38, phospho-Erk 1/2, Erk 1/2, phospho-C/EBP- β (Thr235), and C/EBP- β levels in cell lysates were
611 assessed by western blot. Actin served as the loading control. (B) C/EBP- β knockout THP-1 cell
612 lines (C/EBP- β KO-1 and C/EBP- β KO-2) were infected with ZIKV at 5 MOI. C3 and C/EBP- β
613 proteins in cell lysates were quantitatively analyzed by western blot. Actin served as the loading
614 control. (C–F) THP-1 cells were infected with ZIKV at 5 MOI, followed by treatment with an IL-1R
615 antagonist as indicated (C) or 100 ng/ml (E), or with Diacerein as indicated (D) or 50 μ M (F). C3
616 levels in cell lysates were assessed by western blot (C and D). Actin served as the loading control.
617 Secreted C3 levels in supernatants were measured by ELISA (E and F). Statistically significant
618 differences between the groups were determined using Student's t-test (E and F); ***P < 0.001;
619 ****P < 0.0001. Bars indicate mean \pm SEM.

620 **Fig. 8** ZIKV infection promotes C/EBP- β and C3 expression and activation in the *Ifnar1*^{−/−} mice.
621 *Ifnar1*^{−/−} mice were infected with 10³ PFU of ZIKV (n = 7) or PBS (mock; n = 4 to 7). (A) C/EBP- β
622 mRNA levels in the brain homogenates were determined by RT-qPCR. (B) Phospho-C/EBP- β
623 (Thr188) and C/EBP- β (LAP) protein levels in lysates of the brain homogenates were assessed by
624 western blot. Actin served as the loading control. (C) C3 mRNA levels in the brain homogenates
625 were determined by RT-qPCR. (D) C3 protein levels in lysates of the brain homogenates were
626 assessed by ELISA. (E) C3 protein levels in mouse sera were measured by ELISA. (F) C5a protein

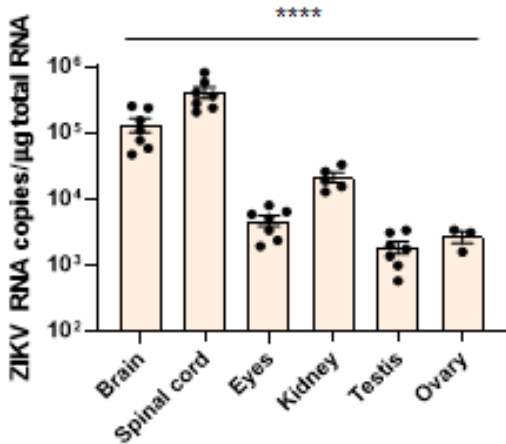
627 levels in lysates of the brain homogenates were quantitatively analyzed by ELISA. Statistically
628 significant differences between the groups were determined using Student's t-test (A, C, D, and F)
629 and one-way analysis of variance (ANOVA; E); *** $P < 0.001$; **** $P < 0.0001$. Bars indicate mean
630 \pm SEM.

631

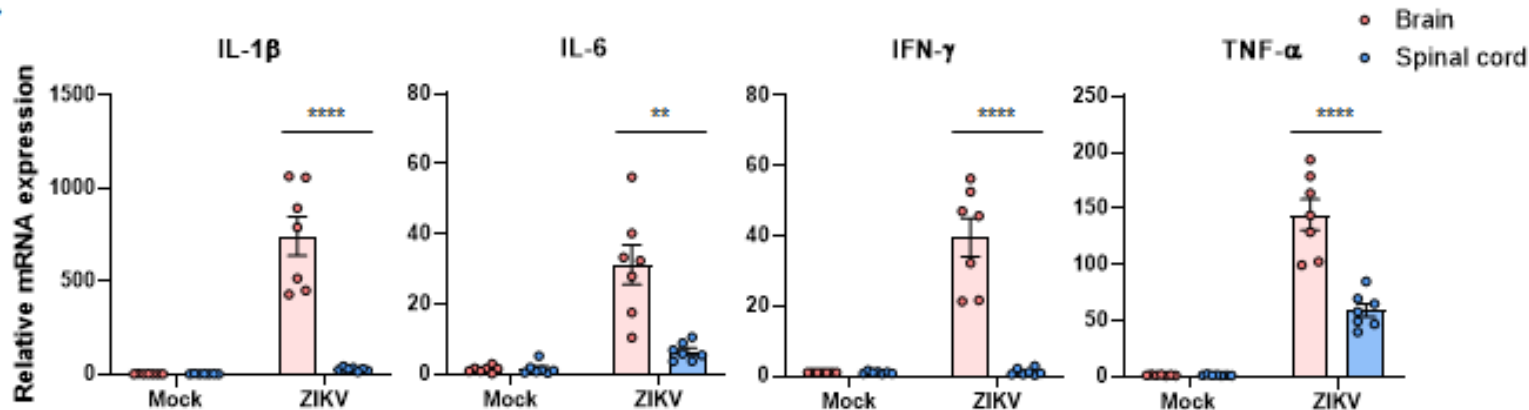
A



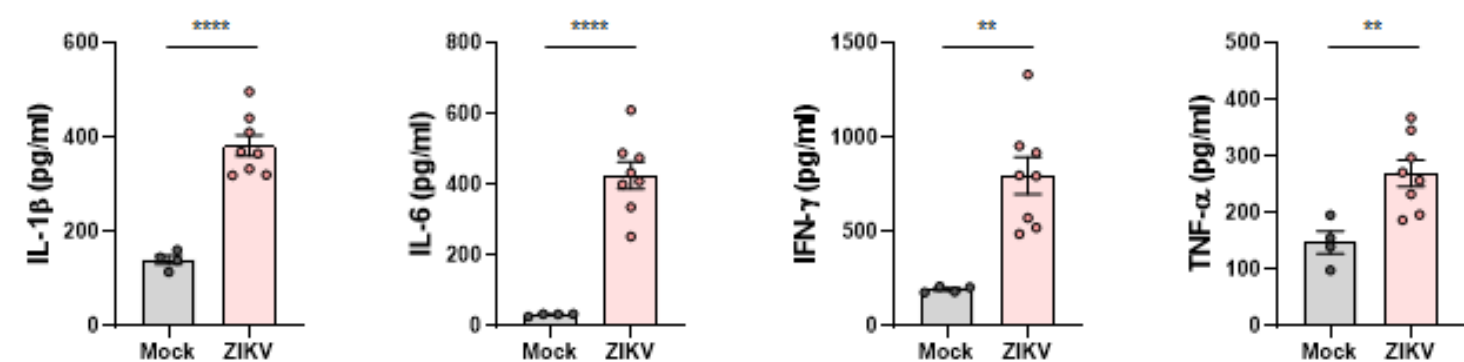
B

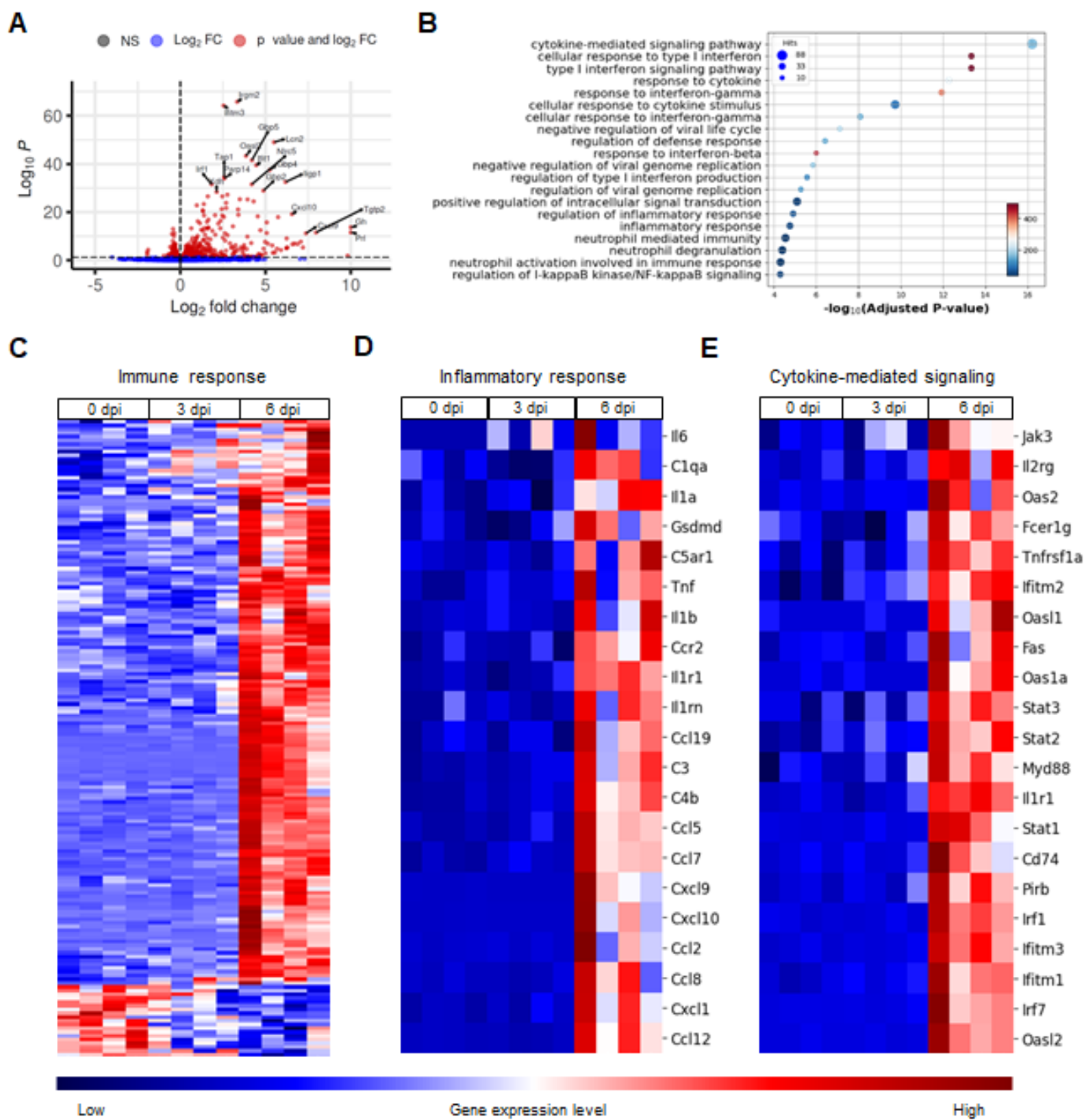


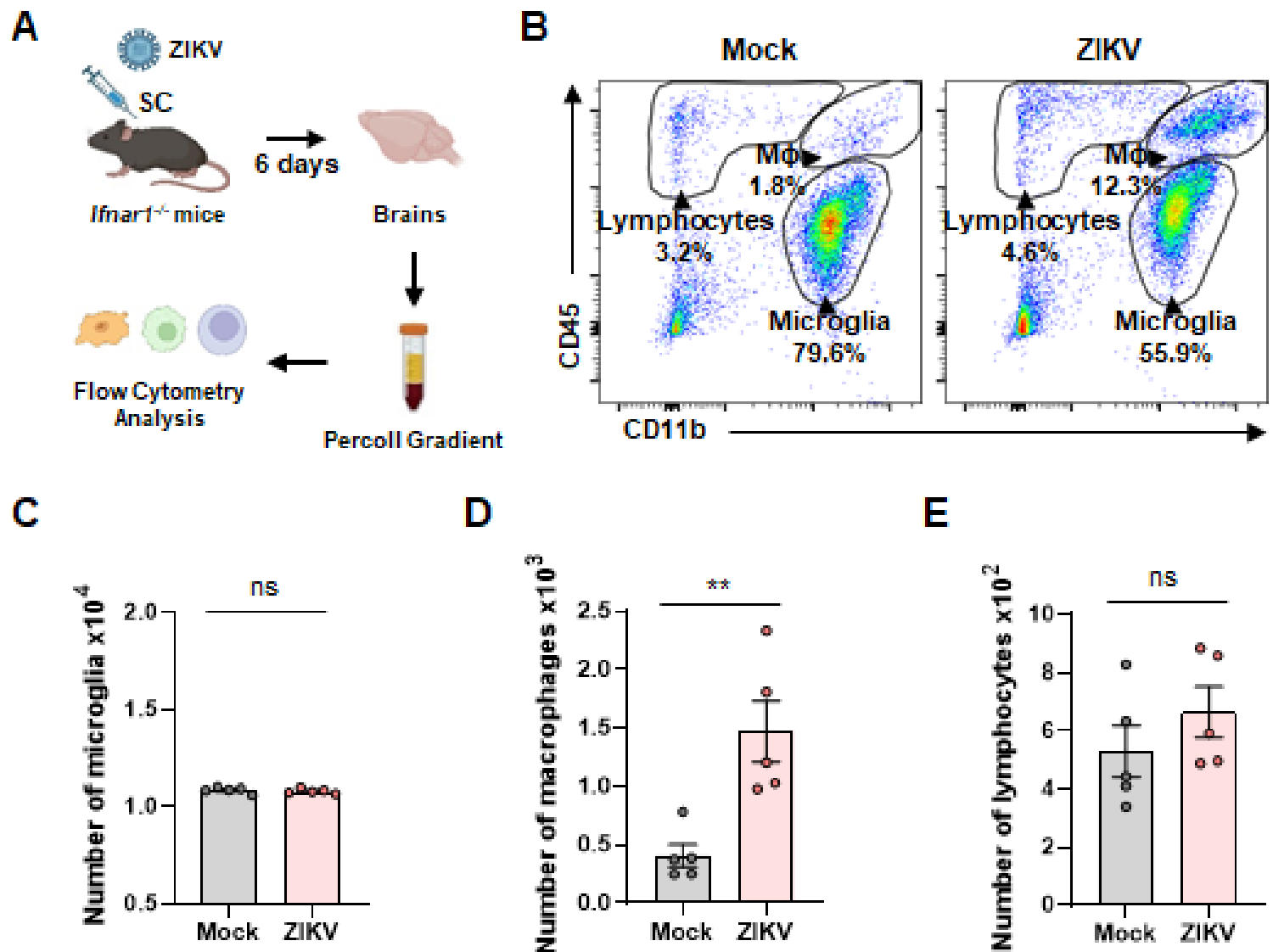
C

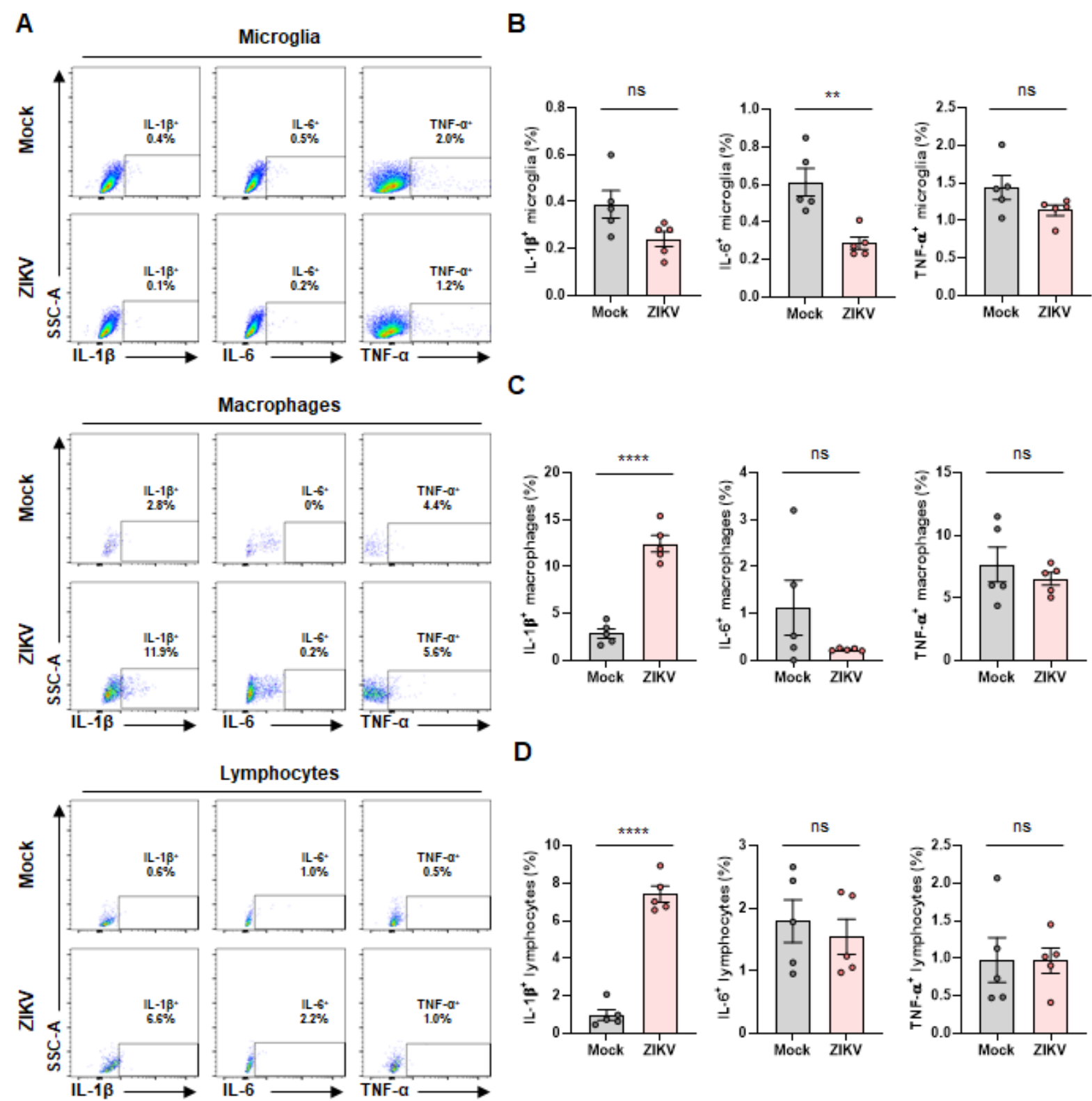


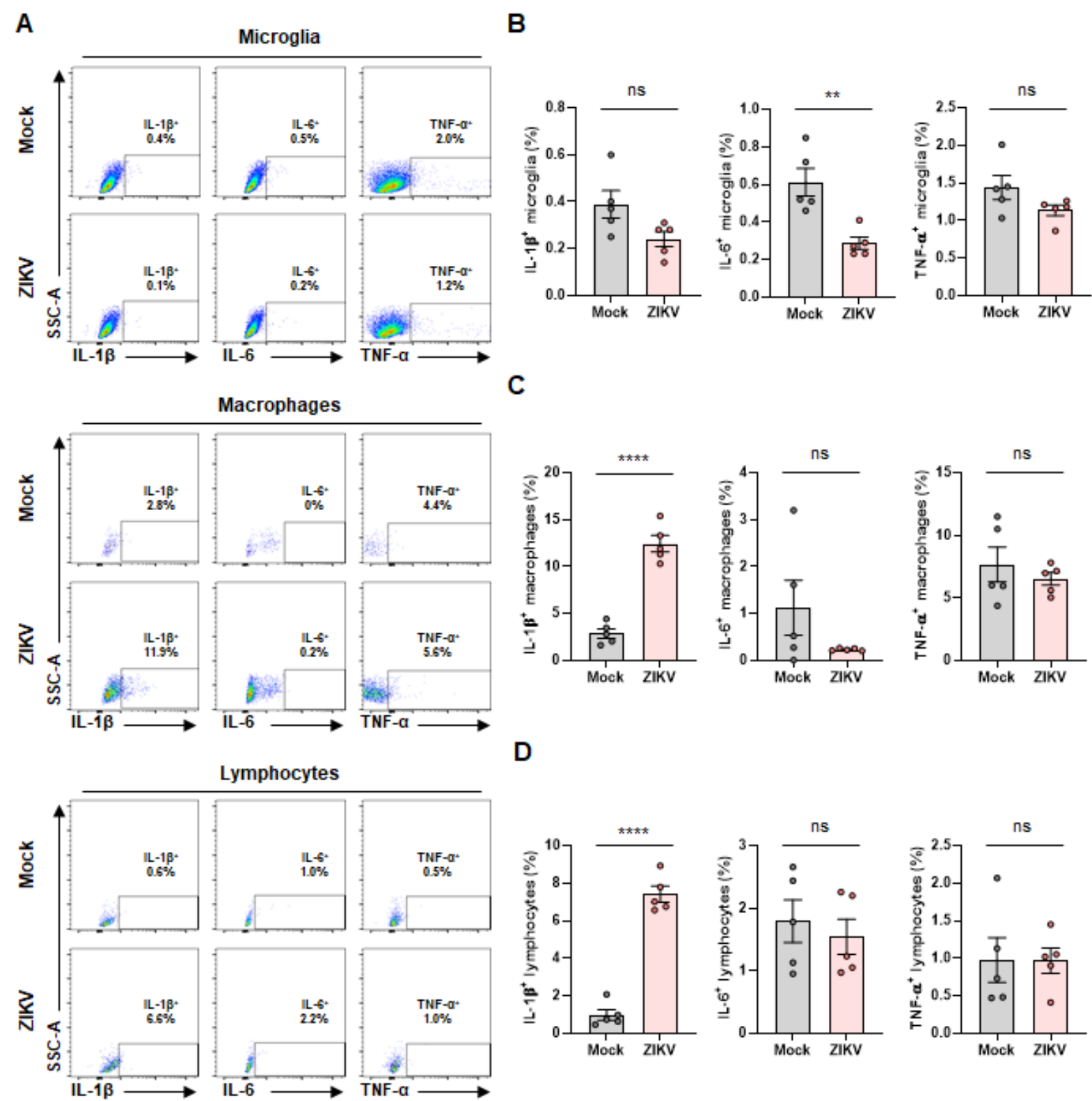
D



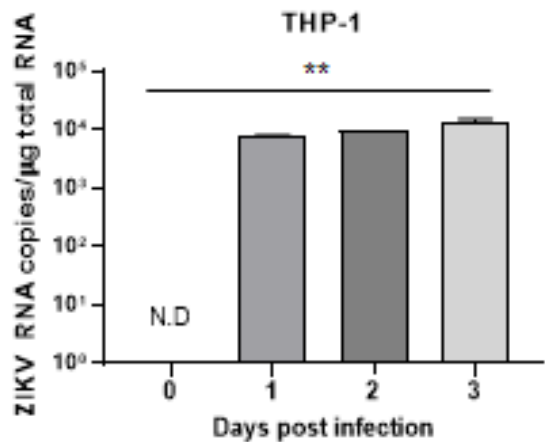




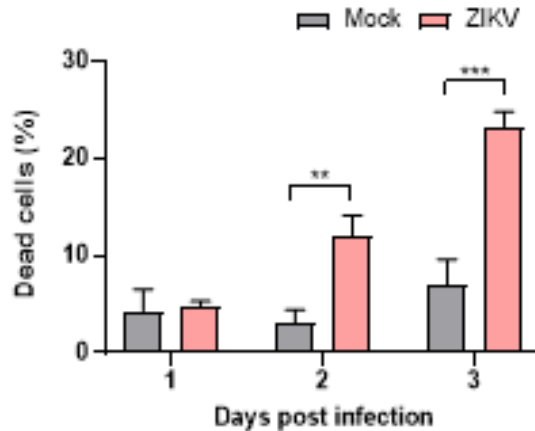




A



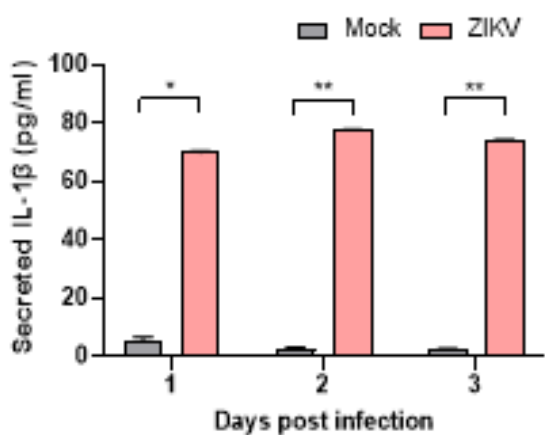
D



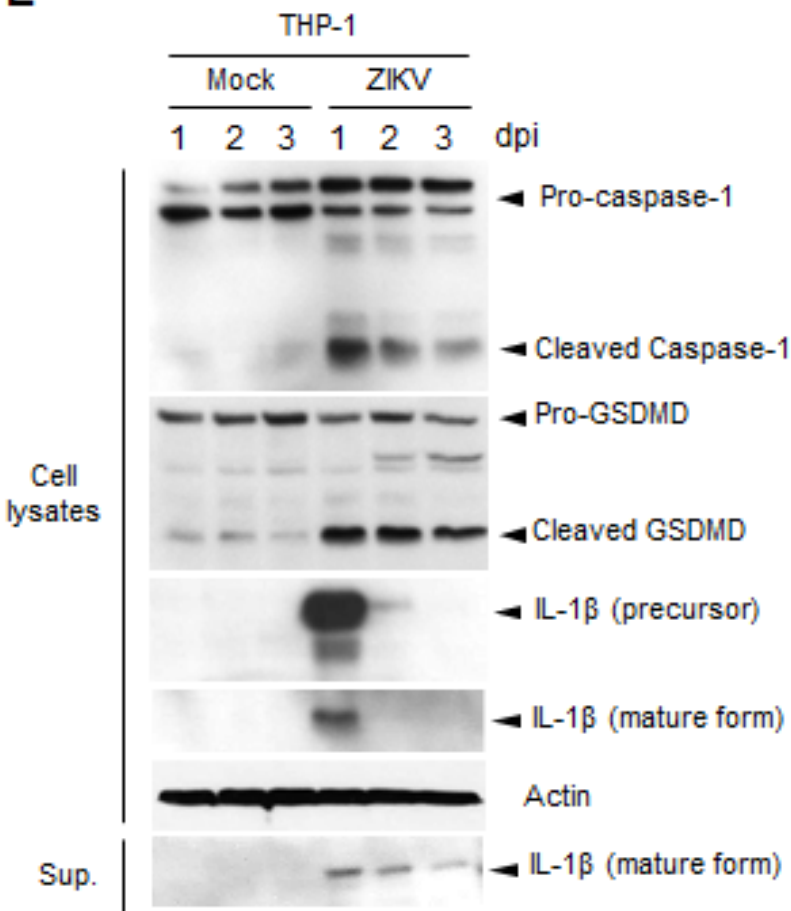
B



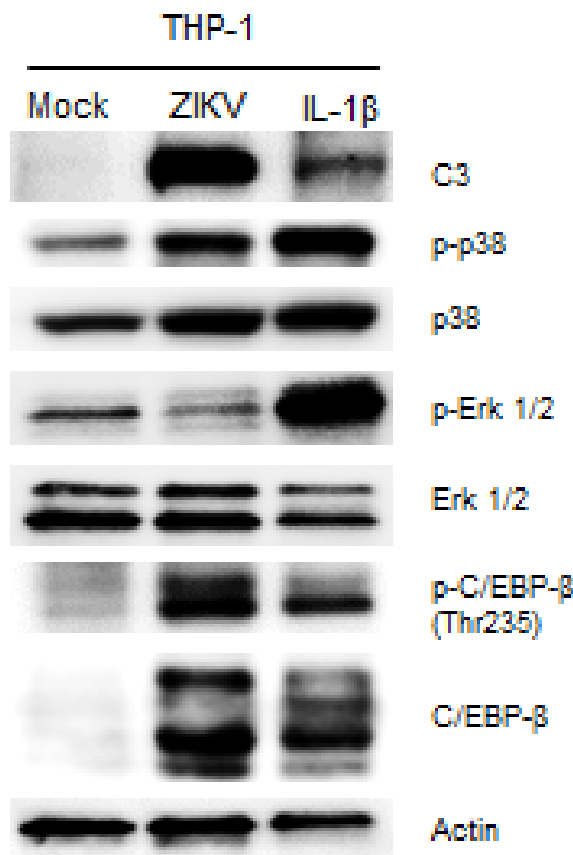
C



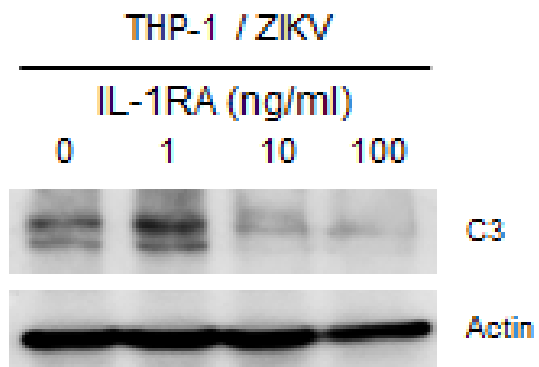
E



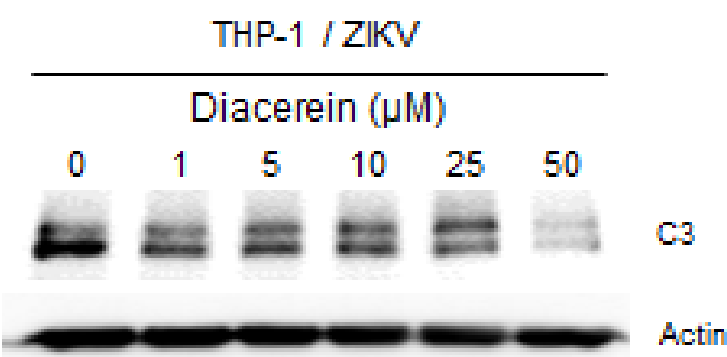
A



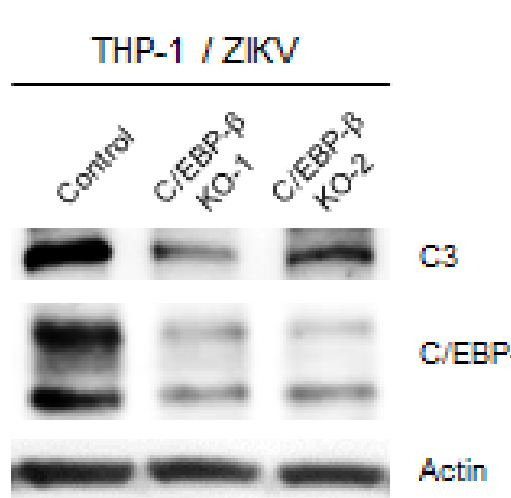
C



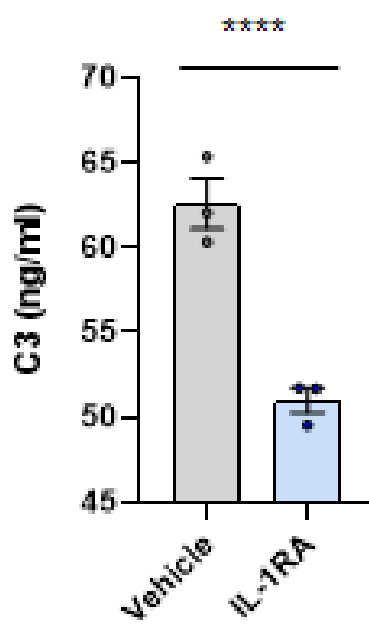
D



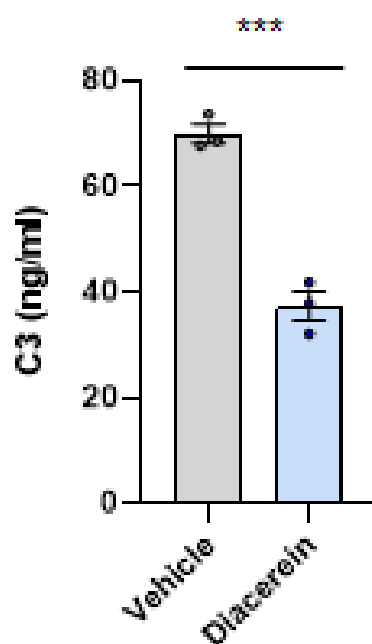
B



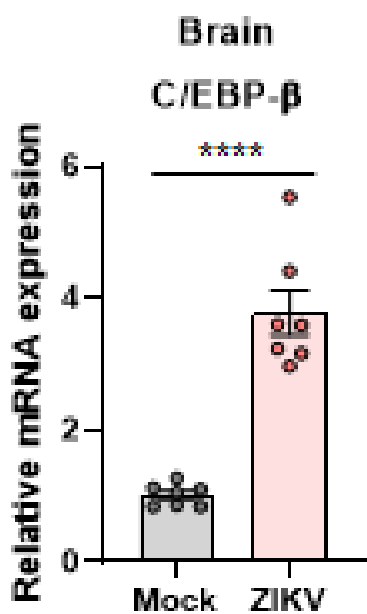
E



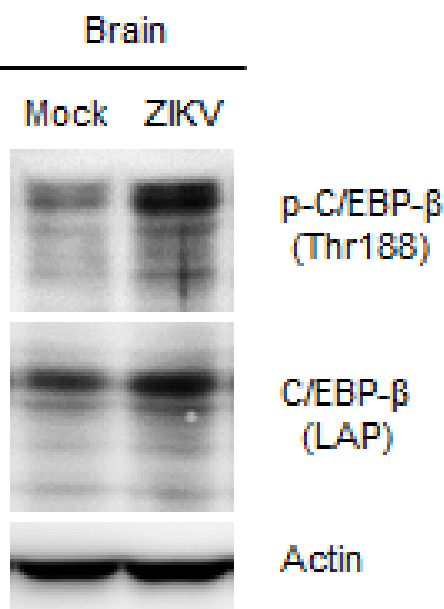
F



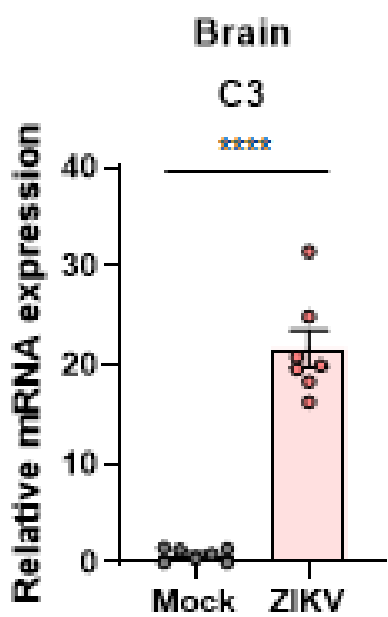
A



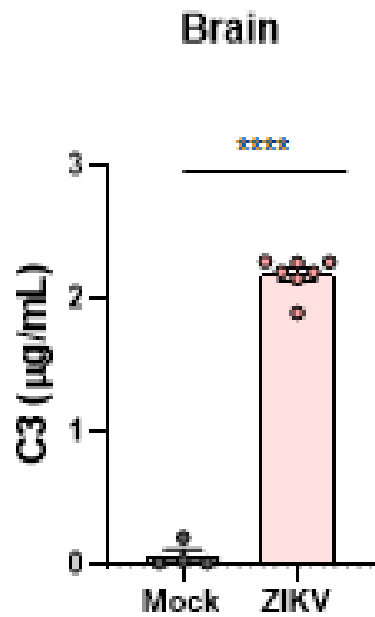
B



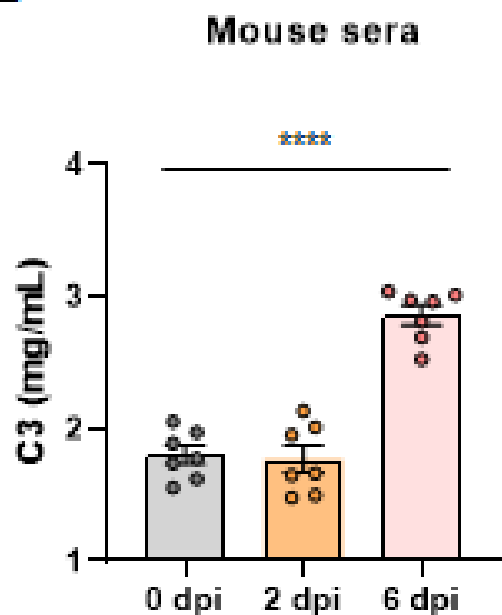
C



D



E



F

